

PFC/JA-80-23

INFLUENCE OF WALL IMPEDANCE ON THE ELECTRON
CYCLOTRON MASER INSTABILITY

H. S. Uhm
Ronald C. Davidson

12/1/80

INFLUENCE OF WALL IMPEDANCE ON THE ELECTRON CYCLOTRON MASER INSTABILITY

Han S. Uhm
Naval Surface Weapons Center
White Oak, Silver Spring, Maryland 20910

Ronald C. Davidson
Plasma Fusion Center
Massachusetts Institute of Technology
Cambridge, Massachusetts 02139

The influence of finite wall impedance on the cyclotron maser instability is investigated for a hollow electron beam. The stability analysis is carried out within the framework of the linearized Vlasov-Maxwell equations, assuming that the beam thickness is much less than the mean radius of the beam. The formal dispersion relation for azimuthally symmetric electromagnetic perturbations is obtained, including the important influence of arbitrary wall impedance. One of the most important features of the analysis is that, for a purely resistive wall, the instability growth rate is substantially reduced by a very small wall resistivity. Moreover, the range of axial wavenumbers corresponding to instability increases rapidly as the wall resistivity is increased. Cyclotron maser stability properties for a dielectric loaded waveguide are also investigated. For appropriate choice of dielectric constant ϵ and thickness of the dielectric material, it is shown that the instability bandwidth can be more than double that for a perfectly conducting waveguide.

I. INTRODUCTION

In recent years, there has been a growing interest in the electron cyclotron maser instability¹⁻⁹ in connection with intense microwave generation.¹⁰⁻¹³ For the most part, previous theoretical analyses of this instability have been carried out without including the influence of finite impedance effects of the waveguide, which has been assumed to be a perfect conductor. Although this is a reasonable assumption in many experiments, we expect a significant modification of the stability behavior when a small amount of resistivity is introduced into the waveguide wall, e.g., to assure stable operation during microwave amplification. Moreover, to increase the bandwidth of microwave amplification, a dielectric loaded waveguide is more desirable than a purely conducting waveguide. However, in a dielectric loaded waveguide, the impedance of the wall is purely reactive. Therefore, in the present article, we investigate the influence of general wall impedance Z on the cyclotron maser instability in a hollow electron beam.

Equilibrium and stability properties are calculated for the specific choice of electron distribution function [Eq. (3)]

$$f_e^0(H, P_\theta, P_z) = (\omega_c N_e / 4\pi^2 mc^2) \delta(\gamma - \hat{\gamma}) \delta(p_z - \hat{p}) \delta(P_\theta - P_0) ,$$

where $H = \gamma mc^2$ is the energy, P_θ is the canonical angular momentum, p_z is the axial momentum, $\omega_c = eB_0 / \gamma mc$ is the electron cyclotron frequency, and N_e is the number of electrons per unit axial length. The stability analysis is carried out within the framework of the linearized Vlasov-Maxwell equations, assuming that the beam thickness is much less than the equilibrium radius R_0 of the beam, and that $v/\hat{\gamma} \ll 1$, where v is Budker's parameter.

The formal stability analysis for azimuthally symmetric electromagnetic perturbations ($\partial/\partial\theta = 0$) is carried out in Sec. II, including the important influence of finite wall impedance Z , which is generally an arbitrary function of the eigenfrequency ω and axial wavenumber k . The dispersion relation (20) for the cyclotron maser instability, when combined with Eqs. (17) and (18), constitutes one of the main results of this paper and can be used to investigate stability properties for a broad range of system parameters. In this regard, we emphasize that Eq. (20) is derived with no a priori assumption that the electron beam is tenuous, or that the wall impedance is independent of ω and k .

In Sec. III, it is shown that the sum of the wave admittances $b_- + b_+$ that occurs in Eq. (20) can be significantly simplified in the limit of a tenuous beam. For $v/\hat{y} \rightarrow 0$, the vacuum transverse electric (TE) mode dispersion relation is given by [Eq. (26)],

$$(\omega^2/c^2 - k^2)R_w^2 = x_{on}^2(\omega, k),$$

where c is the speed of light in vacuo, R_w is the wall radius, x_{on} is the n th root of $Z = J_1(x_{on})/x_{on}J_0(x_{on})$, and $J_\ell(x)$ is the Bessel function of the first kind of order ℓ . The root x_{on} is calculated numerically for a given complex value of wall impedance Z . The detailed dependence of the root x_{on} [Eq. (26)] on eigenfrequency ω and axial wavenumber k is particularly important in connection with the gain and bandwidth for microwave amplification by the cyclotron maser instability.

In Sec. IV, a detailed analytic and numerical investigation of the dispersion relation for the cyclotron maser instability is carried out for a wall impedance Z that is independent of eigenfrequency ω and axial wavenumber k (i.e., $\partial Z/\partial\omega = 0$, $\partial Z/\partial k = 0$). Defining

$Z = |Z|\exp(-i\phi)$, stability properties are investigated for a broad range of impedance magnitude $|Z|$ and phase angle ϕ . One of the most important features of the analysis is that, for a purely resistive wall characterized by $\phi = 90^\circ$, the growth rate is substantially reduced by introducing a very small amount of wall resistivity. This feature represents a general tendency for all radial mode number n . Moreover, the range of the normalized axial wavenumber kc/ω_c corresponding to instability increases rapidly as the wall resistivity is increased.

Cyclotron maser stability properties for a dielectric loaded waveguide are investigated in Sec. V, assuming that the impedance of the dielectric material is purely reactive. It is shown that stability properties exhibit a sensitive dependence on the value of dielectric constant ϵ and the thickness of dielectric material. By appropriate choice of ϵ and thickness of dielectric material, it is shown that the instability bandwidth can be more than double that for a perfectly conducting waveguide. Moreover, the dielectric material reduces the radial wavelength of the waveguide modes, thereby significantly modifying the nature of the perturbations. The influence of beam-induced self-dielectric effects on stability behavior is also investigated. However, for a low density beam ($v/\hat{v} < 0.005$) with small transverse velocity, self-dielectric effects are negligibly small.

II. LINEARIZED VLASOV-MAXWELL EQUATIONS

The equilibrium configuration consists of a hollow relativistic electron beam propagating parallel to a strong, externally applied magnetic field $B_0 \hat{e}_z$. The mean radius of the electron beam is denoted by R_0 , and a finite-impedance wall is located at radius $r = R_w$. Cylindrical polar coordinates (r, θ, z) are introduced. Moreover, in the present analysis, we assume

$$v/\hat{\gamma} \ll 1, \quad (1)$$

where $v = N_e e^2 / mc^2$ is Budker's parameter,

$$N_e = 2\pi \int_0^R c dr n_e^0(r), \quad (2)$$

is the number of electrons per unit axial length. $n_e^0(r)$ is the equilibrium electron density, c is the speed of light in vacuo. $-e$ and m are the electron charge and rest mass, respectively, and $\hat{\gamma}mc^2$ is the characteristic electron energy in the laboratory frame. Consistent with the low-density assumption in Eq. (1), we also neglect the influence of equilibrium self fields.

In the present analysis, we investigate stability properties for the choice of equilibrium distribution function

$$f_e^0(H, P_\theta, P_z) = \frac{\hat{\omega}_c N_e}{4\pi^2 \hat{\gamma} mc^2} \delta(\gamma - \hat{\gamma}) \delta(p_z - \hat{p}) \delta(P_\theta - P_0), \quad (3)$$

where $H = \gamma mc^2 = (m^2 c^4 + c^2 p_\perp^2)^{1/2}$ is the total energy, p_z is the axial momentum, $P_\theta = r[P_\theta - (e/2c)rB_0]$ is the canonical angular momentum, $\hat{\omega}_c = eB_0/mc$ is the nonrelativistic electron cyclotron frequency,

$$P_0 = -(e/2c)(R_0^2 - r_L^2)B_0, \quad (4)$$

is the canonical angular momentum of an electron with Larmor radius,

$$r_L = [(\gamma^2 - 1)c^2/\hat{\omega}_c^2 - (\hat{p}/m\hat{\omega}_c)^2]^{1/2} . \quad (5)$$

and \hat{p} is a constant. For notational convenience, we also introduce the definitions $\beta_z = \hat{p}/\gamma mc$ and $\beta = (1 - \beta_z^2 - 1/\gamma^2)^{1/2}$. Detailed equilibrium properties for the choice of distribution function in Eq. (3) have been discussed previously in the literatures.^{5,7}

In the subsequent stability analysis, use is made of the linearized Vlasov-Maxwell equations for azimuthally symmetric perturbations ($\partial/\partial\theta = 0$) about a tenuous, hollow beam equilibrium described by Eq. (3). We adopt a normal-mode approach in which all perturbations are assumed to vary according to

$$\delta\psi(x,t) = \hat{\psi}(r)\exp[i(kz - \omega t)] ,$$

where $\text{Im}\omega > 0$. Here, ω is the complex eigenfrequency and k is the axial wavenumber. The Maxwell equations for the perturbed electric and magnetic field amplitudes can be expressed as

$$\nabla_{\perp} \times \hat{E}_{\perp}(x) = i(\omega/c)\hat{B}_{\perp}(x) ,$$

$$\nabla_{\perp} \times (1/\mu)\hat{B}_{\perp}(x) = (4\pi/c)\hat{J}_{\perp}(x) - i(\omega/c)\epsilon \hat{E}_{\perp}(x) , \quad (6)$$

where ϵ and μ are the dielectric constant and permeability, respectively, of the wall material, $\hat{E}_{\perp}(x)$ and $\hat{B}_{\perp}(x)$ are the perturbed electric and magnetic fields, and

$$\hat{J}_{\perp}(x) = -e \int d^3p \, x \, \hat{f}_e(x,p) \quad (7)$$

is the perturbed current density. Note that $\epsilon = \mu = 1$ in vacuo.

In Eq. (7),

$$\hat{f}_e(x,p) = e \int_{-\infty}^0 d\tau \exp(-i\omega\tau) \left(\hat{f}_e(x') + \frac{x' \times \hat{B}(x')}{c} \right) \cdot \frac{\partial}{\partial p} f_e^0 \quad (8)$$

is the perturbed distribution function, $\tau = t' - t$, and the particle trajectories $\mathbf{x}'(t')$ and $\mathbf{p}'(t')$ satisfy $d\mathbf{x}'/dt' = \mathbf{v}'$ and $d\mathbf{p}'/dt' = -e\mathbf{v}' \times \mathbf{B}_0 \hat{\mathbf{e}}_z / c$, with "initial" conditions $\mathbf{x}'(t' = t) = \mathbf{x}$ and $\mathbf{v}'(t' = t) = \mathbf{v}$.

Making use of Eq. (6), it is straightforward to show that

$$\begin{aligned}\hat{B}_r(r) &= -(kc/\omega)\hat{E}_\theta(r), \\ \hat{B}_z(r) &= -i(c/\omega r)[\partial(r\hat{E}_\theta)/\partial r],\end{aligned}\quad (9)$$

and

$$\mu \frac{\partial}{\partial r} \left(\frac{1}{\mu r} \frac{\partial}{\partial r} (r\hat{E}_\theta) \right) + p^2 \hat{E}_\theta = -\frac{4\pi i \omega \mu}{c} \hat{J}_\theta, \quad (10)$$

where

$$p^2 = \omega^2 \mu \epsilon / c^2 - k^2, \quad (11)$$

\hat{E}_θ is the azimuthal component of the perturbed electric field, and \hat{B}_r and \hat{B}_z are the radial and axial components, respectively, of the perturbed magnetic field. The field equations (9) and (10) yield the familiar transverse electric (TE) waveguide modes. For the cyclotron maser instability, it is well established^{1,9} that the beam cyclotron resonance mode couples much more strongly with the TE waveguide mode than with the transverse magnetic (TM) waveguide mode. Therefore, the present analysis is restricted to the TE mode polarization.

The perturbed azimuthal electric field $\hat{E}_\theta(r)$ is continuous across inner and outer boundaries ($r = R_1$ and $r = R_2$) of the electron beam. Integrating Eq. (10) from $r = R_1 - \delta$ to $r = R_2 + \delta$, and taking the limit $\delta \rightarrow 0_+$, we obtain the approximate result¹

$$\hat{B}_z(R_2^+) - \hat{B}_z(R_1^-) = -\frac{4\pi}{c} \int_{R_1^-}^{R_2^+} dr \hat{J}_\theta(r), \quad (12)$$

where $\psi(R_2^\pm)$ denotes $\lim_{\delta \rightarrow 0_+} \psi(R_2 \pm \delta)$, and use has been made of the thin beam approximation. For convenience, in the subsequent analysis we

introduce the normalized magnetic wave admittance¹ b_{\pm} defined at the inner and outer surfaces of the electron beam by

$$b_{-} = -i(\omega/p_1^2 c R_0) \hat{B}_z(R_1^-) / \hat{E}_{\theta}(R_0) , \quad (13)$$

$$b_{+} = i(\omega/p_1^2 c R_0) \hat{B}_z(R_2^+) / \hat{E}_{\theta}(R_0) ,$$

where

$$p_1^2 = \omega^2 / c^2 - k^2 . \quad (14)$$

Moreover, we also define the wave impedance $Z(\omega, k)$ of the wall as

$$Z(\omega, k) = -i(c/\omega R_w) \hat{E}_{\theta}(R_w) / \hat{B}_z(R_w) , \quad (15)$$

where R_w is the wall radius.

Since the perturbed current density vanishes in the vacuum regions inside and outside the beam, it is evident that the solutions to Eq. (10) in the vacuum regions are given by

$$\hat{E}_{\theta}(r) = \begin{cases} A J_1(p_1 r), & r < R_1 , \\ B J_1(p_1 r) + C N_1(p_1 r), & R_2 < r < R_w , \end{cases} \quad (16)$$

where $J_{\ell}(p_1 r)$ and $N_{\ell}(p_1 r)$ are Bessel functions of the first and second kind, respectively, of order ℓ . Making use of Eqs. (15) and (16), and the thin beam approximation ($R_1 \approx R_2 \approx R_0$), we express the sum of wave admittances in Eq. (13) as

$$b_{-} + b_{+} = \frac{[2g(\xi)/\pi](R_w/R_0\xi)^2}{J_1(\xi R_0/R_w)[J_1(\xi R_0/R_w) + g(\xi)N_1(\xi R_0/R_w)]} , \quad (17)$$

where $\xi = p_1 R_w$, and

$$g(\xi) = \frac{\xi J_0(\xi)}{N_1(\xi) - \xi Z N_0(\xi)} \left(Z - \frac{J_1(\xi)}{\xi J_0(\xi)} \right) . \quad (18)$$

Substituting Eq. (13) into Eq. (12) gives

$$(b_- + b_+) = -i \frac{4\pi\omega R_w^2}{c^2 \xi^2 R_0 \hat{E}_\theta(R_0)} \int_{R_1^-}^{R_2^+} dr \hat{J}_\theta(r) . \quad (19)$$

After some tedious but straightforward algebraic manipulation that makes use of Eqs. (7), (8), and (9), we obtain the dispersion relation for the cyclotron maser instability,

$$b_- + b_+ = - \frac{v \beta_1^2}{2 \hat{\gamma} \xi^2} \left(\frac{R_w}{R_0} \right)^2 \frac{\omega^2 - k^2 c^2}{(\omega - k \beta_z c - \omega_c)^2} , \quad (20)$$

where $\omega_c = \hat{\omega}_c / \hat{\gamma}$ is the electron cyclotron frequency in the laboratory frame, and use has been made of $\beta_1^2 \ll 1$. For a detailed derivation of Eq. (20), the reader is urged to review the previous literatures.^{1,3,5}

In the remainder of this article, we make use of Eq. (20) to investigate cyclotron maser stability properties for various values of wall impedance Z in Eq. (18).

III. TENUOUS BEAM LIMIT

To simplify the expression for $b_- + b_+$ in Eq. (17), it is useful to consider the limit where the beam is very tenuous, i.e.,

$$v/\hat{\gamma} \rightarrow 0 . \quad (21)$$

In this limit, the vacuum TE mode dispersion relation is given by

$$Z = J_1(\xi)/\xi J_0(\xi) , \quad (22)$$

where $Z(\omega, k)$ is the wave impedance of the wall [Eq. (15)], and ξ is defined by $\xi = (\omega^2/c^2 - k^2)^{1/2} R_w$. Substituting Eq. (22) into Eq. (18), and making use of Eq. (17) gives the simplified expression

$$b_- + b_+ = - \left(\frac{R_w J_0(\xi)}{R_0 J_1(\xi R_0/R_w)} \right)^2 \left(Z - \frac{J_1(\xi)}{\xi J_0(\xi)} \right) . \quad (23)$$

For convenience in the subsequent analysis, we denote the n th root of Eq. (22) by

$$\xi = x_{on}(\omega, k) = x_r(\omega, k) + i x_i(\omega, k) , \quad (24)$$

for a specified value of wall impedance

$$Z = |Z| \exp(-i\phi) = Z_r + iZ_i . \quad (25)$$

For a very tenuous beam [Eq. (21)], it is evident from Eqs. (22) and (24) that

$$(\omega^2/c^2 - k^2) R_w^2 = x_{on}^2(\omega, k) , \quad (26)$$

is a good approximation to the dispersion relation in Eq. (20). The right-hand side of Eq. (20) describes the beam-produced modifications to the vacuum dispersion relation (26). We remind the reader that the root x_{on} is generally a function of the eigenfrequency ω and axial

wavenumber k . For an impedance satisfying $|Z| \ll 1$, we obtain

$$x_{on} = \alpha_{on} [1 + |Z| \exp(-i\phi)] , \quad (27)$$

from Eqs. (22) and (25). Therefore, the vacuum waveguide mode for zero wall impedance can be expressed as

$$(\omega^2/c^2 - k^2) R_w^2 = \alpha_{on}^2 , \quad (28)$$

where α_{on} is the n th root of $J_1(\alpha_{on}) = 0$, which is independent of ω and k .

Shown in Fig. 1 are contours of constant phase angle ϕ and modulus $|Z|$ of the function $Z = J_1(x_{on})/x_{on} J_0(x_{on})$ in the complex plane $x_{on} = x_r - ix_i$, for (a) $n = 1$ and (b) $n = 2$. We note from Fig. 1 that the n th root x_{on} of Eq. (22) approaches α_{on} as the magnitude of the wall impedance is reduced to zero, $|Z| \rightarrow 0$. On the other hand, x_{on} approaches β_{on} as $|Z|$ increases to infinity. Here β_{on} is the n th root of $J_0(\beta_{on}) = 0$. For specified values of $|Z|$ and ϕ , we note that $x_{on} = x_r - ix_i$ can be determined from Fig. 1. For example, for $|Z| = 0.3$, $\phi = 90^\circ$, and $n = 1$, it follows from Fig. 1 that $x_r = 3.12$ and $x_i = 0.82$. Evidently, the root x_{on} is generally a very complicated function of the wall impedance Z .

The dependence of x_{on} on frequency ω and axial wavenumber k has a particularly important effect on the gain and bandwidth of microwave amplification by the cyclotron maser instability. Shown in Fig. 2 are plots of $\omega = (k^2 c^2 + \alpha_{on}^2 c^2 / R_w^2)^{1/2}$ versus k corresponding to zero wall impedance, and $\omega = (k^2 c^2 + x_{on}^2 c^2 / R_w^2)^{1/2}$ versus k corresponding to an arbitrary wall impedance. The straight line $\omega = k\beta_z c + \omega_c$ represents the cyclotron resonance mode. It is important to note from Fig. 2 that the interaction region of the cyclotron resonance mode

with the vacuum waveguide dispersion relation is increased substantially by appropriate choice of the wall impedance (x_{on}). In general, we conclude that the growth rate and bandwidth of the cyclotron maser instability can be enhanced considerably if the functional dependence of the wall impedance on ω and k is properly matched with the cyclotron resonance mode over a broad region of k space. To make quantitative estimates, however, a detailed investigation of the wall impedance is required. Previous studies¹⁴ indicate that properly chosen waveguide structures will provide the necessary wall impedance. In this regard, the influence of nonuniform wall impedance on the cyclotron maser instability is currently under investigation by the authors for a wide range of parameters and waveguide structures. As a simple illustrative example, in Sec. V we examine cyclotron maser stability properties for the case of dielectric loaded waveguide.

IV. CYCLOTRON MASER INSTABILITY FOR CONSTANT WALL IMPEDANCE

In this section, we investigate cyclotron maser stability properties for a hollow electron beam assuming that the wall impedance is independent of frequency ω and the wavenumber k , i.e.,

$$\partial Z / \partial \omega = 0, \quad \partial Z / \partial k = 0. \quad (29)$$

Taylor expanding Eq. (23) about $(\omega^2/c^2 - k^2)R_w^2 = x_{on}^2$, it is straightforward to show that $b_- + b_+$ can be approximated by

$$b_- + b_+ = -\frac{R_w^2}{2x_{on}^2} \left(\frac{R_w}{R_0} \right)^2 \frac{J_1^2(x_{on}) - J_0(x_{on})J_2(x_{on})}{J_1^2(x_{on}R_0/R_w)} \left(\frac{\omega^2}{c^2} - k^2 - \frac{x_{on}^2}{R_w^2} \right). \quad (30)$$

Substituting Eq. (30) into Eq. (20), and making use of Eq. (24), we obtain the approximate dispersion relation

$$\frac{\omega^2}{c^2} - k^2 - \frac{x_{on}^2}{R_w^2} = -\frac{v\beta_1^2}{\gamma R_w^2} \frac{J_1^2(x_{on}R_0/R_w)}{J_1^2(x_{on}) - J_0(x_{on})J_2(x_{on})} - \frac{\omega^2 - k^2c^2}{(\omega - k\beta_z c - \omega_c)^2}, \quad (31)$$

for a thin, tenuous beam. A stability analysis of Eq. (31) is carried out in the remainder of this section for a broad range of physical parameters.

In order to investigate the influence of wall resistivity on stability behavior, we examine Eq. (31) for the case of small wall impedance with $|Z| \ll 1$. In this limit, it is convenient to choose the wall radius R_w according to

$$R_w = \alpha_{on} c / \omega_c \gamma_z, \quad (32)$$

where γ_z is defined by $\gamma_z^2 = (1 - \beta_z^2)^{-1}$. Equation (32) assures that the group velocity of the $|Z| = 0$ vacuum waveguide mode

is equal to the beam velocity at a certain value of wavenumber k . Making use of Eq. (32), and defining the normalized Doppler-shifted eigenfrequency χ by

$$\chi = (\omega - k\beta_z c - \omega_c) / \omega_c, \quad (33)$$

it is straightforward to show that the dispersion relation in Eq. (31) can be expressed as

$$\begin{aligned} \chi^4 + 2 \left(\frac{k\beta_z c}{\omega_c} + 1 \right) \chi^3 + \left[\left(\frac{k\beta_z c}{\omega_c} + 1 \right)^2 - \left(\frac{kc}{\omega_c} \right)^2 - \left(\gamma_z \frac{x_{on}}{\alpha_{on}} \right)^2 \right] \chi^2 \\ + \frac{\nu}{\gamma} \left(\gamma_z \beta_z \frac{x_{on}}{\alpha_{on}} \right)^2 \frac{J_1^2(x_{on} R_o/R_w)}{J_1^2(x_{on}) - J_0(x_{on})J_2(x_{on})} = 0. \end{aligned} \quad (34)$$

The normalized growth rate $\chi_i = \text{Im}\chi$ and Doppler-shifted real frequency $\chi_r = \text{Re}\chi$ have been calculated numerically from Eq. (34) for $\nu = 0.002$, $\hat{\gamma} = 1.118$, $\beta_z = 0.4$, and several values of wall impedance Z . For a specified value of Z , the root x_{on} is determined from Fig. 1. For example, we find from Fig. 1 that $x_{on} = (x_r, x_i) = (3.82, 0.167)$ for $Z = (|Z|, \phi) = (0.045, 90^\circ)$.

Although present experiments on the cyclotron maser instability are carried out in highly conducting cylindrical waveguides, it is necessary to investigate stability properties for a resistive waveguide, since a small wall resistivity is sometimes required for stable operation as a microwave amplifier. In this regard, we investigate the dispersion relation in Eq. (34) for a purely resistive wall characterized by $\phi = 90^\circ$. Shown in Fig. 3 are plots of (a) normalized growth rate χ_i and (b) normalized Doppler-shifted real frequency χ_r versus kc/ω_c obtained from Eq. (34) for $n = 1$, $R_o/R_w = 0.5$, $\phi = 90^\circ$, and several values of $|Z|$. In Fig. 3(b), χ_r is plotted only for the ranges of kc/ω_c corresponding to instability ($\chi_i \geq 0$). Several

features are noteworthy from Fig. 3. First, the maximum growth rate decreases as the wall impedance $|Z|$ is increased. Indeed, the growth rate is substantially reduced by introducing a very small amount of wall resistivity. As evident from Eq. (34) and Fig. 1, this feature represents a general tendency for all radial mode numbers n . Second, the range of kc/ω_c corresponding to instability increases rapidly as the resistivity of the wall is increased. That is, the bandwidth for microwave amplification increases. Third, for a lossless conductor, the Doppler-shifted real frequency increases abruptly when the wavenumber k approaches the values corresponding to marginal stability ($\chi_1=0$). For a resistive wall, however, the variations in χ_r are less abrupt [Fig. 3(b)].

The dependence of stability properties on phase angle ϕ is illustrated in Fig. 4, where the normalized growth rate χ_1 is plotted versus kc/ω_c for $n=1$, $R_o/R_w = 0.5$, $|Z| = 0.05$, and several values of ϕ . The Doppler-shifted real frequency is similar in form to Fig. 3(b), and is not illustrated in Fig. 4. From Fig. 4, it is evident that the maximum growth rate occurs for $\phi = 180^\circ$. For the particular impedance magnitude ($|Z| = 0.05$) chosen in Fig. 4, the instability growth rate decreases abruptly as the phase angle ϕ approaches zero.

To investigate the cyclotron maser instability for a purely reactive impedance¹⁵ characterized by $\phi = 0^\circ$ or $\phi = 180^\circ$, we analyze the dispersion relation in Eq. (31) for different values of x_{on} with $x_1 = 0$. In order to maximize the growth rate and efficiency of microwave amplification, we choose³

$$R_w = x_{on} c/\omega_c \gamma_z, \quad R_o/R_w = \alpha_{11}/x_{on}, \quad (35)$$

where α_{11} is the first root of $J_1'(\alpha_{11}) = 0$ and $J_1'(x) = dJ_1/dx$. Making

use of Eqs. (33) and (35), it can be shown that Eq. (31) reduces to

$$\begin{aligned} \chi^4 + 2 \left(\frac{k\beta_z c}{\omega_c} + 1 \right) \chi^3 + \left[\left(\frac{k\beta_z c}{\omega_c} + 1 \right)^2 - \left(\frac{kc}{\omega_c} \right)^2 - \gamma_z^2 \right] \chi^2 \\ + \frac{\nu}{\hat{\gamma}} \left(\frac{\gamma_z^2 \beta_z}{x_{on}} \right)^2 \frac{J_1^2(\alpha_{11})}{J_1^2(x_{on}) - J_0(x_{on})J_2(x_{on})} = 0. \end{aligned} \quad (36)$$

In Fig. 5, the normalized maximum growth rate (solid curve) and R_o/R_w (dashed curve) obtained from Eqs. (36) and (35) are plotted versus $x_{on} = x_r$ for $\nu = 0.002$, $\hat{\gamma} = 1.118$, and $\beta_z = 0.4$. A numerical analysis of Eq. (36) shows that the maximum growth rate occurs for axial wavenumber $k \approx 0.15 \omega_c/c$, for x_{on} in the range $2 \leq x_{on} \leq 4$. We note from Fig. 5 that the instability growth rate increases substantially as x_{on} is reduced to two. Moreover, it may be possible that the growth rate can be increased further by reducing the value x_{on} below two, and by suitably adjusting the beam radius [Eqs. (31) and (36)].

V. CYCLOTRON MASER INSTABILITY FOR A DIELECTRIC LOADED WAVEGUIDE

In this section, we investigate cyclotron maser stability properties for a hollow electron beam in a dielectric loaded waveguide. As illustrated in Fig. 6, the electron beam propagates through a cylindrical waveguide loaded with dielectric material in the range $R_w < r < R_c$. A grounded cylindrical conducting wall is located at radius R_c . In general, the permeability μ of a dielectric material differs from unity by only a few parts in 10^5 ($\mu > 1$ for paramagnetic substances, $\mu < 1$ for diamagnetic substances). Therefore, we approximate $\mu = 1$ in the remainder of this section. In this regard, the perturbed azimuthal electric field $\hat{E}_\theta(r)$ and axial magnetic field $\hat{B}_z(r)$ are continuous across the dielectric boundary at $r = R_w$. From Eq. (10), we obtain

$$\frac{\partial}{\partial r} \left(\frac{1}{r} \frac{\partial}{\partial r} (r \hat{E}_\theta) \right) + p_2^2 \hat{E}_\theta = 0, \quad (37)$$

inside the dielectric material. Here, p_2 is defined by

$$p_2^2 = \omega^2 \epsilon / c^2 - k^2. \quad (38)$$

The solution to Eq. (37) can be expressed as

$$\hat{E}_\theta(r) = A [J_1(p_2 r) - J_1(\zeta) N_1(p_2 r) / N_1(\zeta)], \quad (39)$$

where A is an arbitrary constant and $\zeta = R_c p_2 = R_c (\omega^2 \epsilon / c^2 - k^2)^{1/2}$.

Note that Eq. (39) satisfies the boundary condition $\hat{E}_\theta(r=R_c) = 0$.

Substituting Eq. (39) into Eq. (9), and making use of the boundary conditions at $r = R_w$, we obtain the impedance

$$Z(\omega, k) = \frac{J_1(\eta) N_1(\zeta) - J_1(\zeta) N_1(\eta)}{\eta [J_0(\eta) N_1(\zeta) - J_1(\zeta) N_0(\eta)]}, \quad (40)$$

from the definition in Eq. (17). In Eq. (40), the parameter η is

defined by $\eta = R_w p_2 = R_w (\omega^2 \epsilon / c^2 - k^2)^{1/2}$. Note from Eq. (40) that the wall impedance for a dielectric loaded waveguide is a function of eigenfrequency ω and axial wavenumber k . Since the dielectric constant ϵ is always greater than unity, it follows from Eqs. (14) and (38) that $p_2 > p_1$. We therefore conclude from the definitions $\xi = p_1 R_w$, $\eta = p_2 R_w$, and $\zeta = p_2 R_c$, that

$$R_w / R_c = \eta / \zeta, \quad (41)$$

and

$$\xi \leq \eta \leq \zeta. \quad (42)$$

Equation (20), when combined with Eqs. (17), (18), and (40), yields a closed dispersion relation for the cyclotron maser instability in a dielectric loaded waveguide.

A previous analysis¹ indicates that the maximum growth rate occurs for $b_- + b_+ \approx 0$ and is characterized by the vacuum TE mode dispersion relation [Eq. (22)] in the region $0 \leq r < R_w$. Making use of the definitions $\xi = p_1 R_w$, $\eta = p_2 R_w$, and $\zeta = p_2 R_c$, we can express the vacuum TE mode dispersion relation in Eq. (22) as

$$\omega^2 / c^2 - k^2 = x_{on}^2 / R_w^2 = \xi^2 / R_w^2 = (\xi \zeta / \eta)^2 / R_c^2, \quad (43)$$

where the parameter ξ is related to η by

$$Z = J_1(\xi) / \xi J_0(\xi) = \frac{J_1(\eta) N_1(\zeta) - J_1(\zeta) N_1(\eta)}{\eta [J_0(\eta) N_1(\zeta) - J_1(\zeta) N_0(\eta)]}, \quad (44)$$

for a specified value of ζ . It is instructive to examine Eq. (43)

in the limit $\epsilon \rightarrow 1$. Making use of $\xi = \eta$, and Eq. (44), we obtain

$$(\omega^2 / c^2 - k^2) R_c^2 = \alpha_{on}^2 \text{ from Eq. (43) for } \epsilon = 1.$$

Figure 7 shows a plot of the impedance Z versus ξ (dashed curves) and Z versus η (solid curves) obtained from Eq. (44) for $\zeta = 4, 5$, and 6 .

The horizontal scale in Fig. 7 represents both ξ and η . The solid curves are plotted only for the ranges of η satisfying Eq. (42). Note that for specified values of ξ and ζ , the parameter η is determined from Fig. 7. For example, for $\xi = 2$, we find from Fig. 7 that $\eta = 2.175$ for $\zeta = 4$, $\eta = 3.3$ for $\zeta = 5$, and $\eta = 4.35$ for $\zeta = 6$, which corresponds to the wave impedance $Z = 1.25$ at the surface of the dielectric material. In this particular example ($\xi = 2$), the values of the parameters $\xi\zeta/\eta$ and R_w/R_c are given by $(\xi\zeta/\eta, R_w/R_c) = (3.68, 0.54)$ for $\zeta = 4$, $(3.03, 0.66)$ for $\zeta = 5$, and $(2.70, 0.73)$ for $\zeta = 6$. From the definitions of ξ , η , and ζ , we obtain $\omega^2(\epsilon - 1) = c^2(1 - \xi^2/\eta^2)\zeta^2/R_c^2$, which explicitly demonstrates the strong dependence of the vacuum waveguide eigenfrequency on the dielectric constant ϵ . However, the maximum growth rate of the cyclotron maser instability for an electron beam with $\beta_z^2 \ll 1$ occurs for eigenfrequency ω satisfying $\omega^2 \gg k^2 c^2$. Therefore, in the region of maximum growth, we approximate $\eta^2/\xi^2 = p_2^2/p_1^2$ by

$$\epsilon = \eta^2/\xi^2. \quad (45)$$

In this regard, we can determine the dielectric constant ϵ from Fig. 7 and Eq. (45) in the region of interest for the cyclotron maser instability. As an example, for $\xi = 2$, we obtain $\epsilon = 1.19$ for $\zeta = 4$, $\epsilon = 2.62$ for $\zeta = 5$, and $\epsilon = 4.75$ for $\zeta = 6$. We also emphasize that the impedance Z in Eq. (40) is purely reactive [i.e., $Z_1 = 0$ where Z_1 is defined in Eq. (25)] for eigenfrequency ω satisfying $\omega^2 > k^2 c^2$.

In order to complete the cyclotron maser stability analysis for a dielectric loaded waveguide, it is necessary to numerically solve the dispersion relation in Eq. (20) with no a priori assumption that the beam is very tenuous. However, use is made of the fact that

the Doppler-shifted eigenfrequency $\omega - k\beta_z c - \omega_c$ is well removed from cyclotron resonance, i.e., $|\omega - k\beta_z c - \omega_c| \ll \omega_c$. Evaluating the parameters ξ , η , ζ , and the wave admittance $b_- + b_+$ at $\omega = \omega_0 = k\beta_z c + \omega_c$, the dispersion relation in Eq. (20) can be approximated by

$$\left(\omega_c \frac{d}{d\omega} (b_- + b_+) \right)_{\omega_0} \chi^3 + (b_- + b_+)_{\omega_0} \chi^2 + \frac{\nu}{2\hat{\gamma}} \frac{\beta_z^2}{\xi_0^2} \left(\frac{R_w}{R_0} \right)^2 \times [(1 + \beta_z kc/\omega_c)^2 - (kc/\omega_c)^2] = 0, \quad (46)$$

where $\xi_0 = \xi(\omega = \omega_0)$, and χ is defined in Eq. (33). The normalized growth rate $\chi_1 = \text{Im}\chi$ has been evaluated numerically from Eq. (46) for a broad range of system parameters kc/ω_c , $R_w \omega_c/c$, $R_c \omega_c/c$, and dielectric constant ϵ . In the numerical analysis, it is assumed that the beam parameters are given by $\nu = 0.002$, $\hat{\gamma} = 1.118$ and $\beta_z = 0.4$. Moreover, to maximize the instability growth rate, it is also assumed³ that $R_0 \omega_c/c = \alpha_{11}$, where α_{11} is the first zero of $J_1'(\alpha_{11}) = 0$.

Figure 8 illustrates the influence of self-dielectric effects of the electron beam on the cyclotron maser instability. Shown in Fig. 8 are plots of normalized growth rate χ_1 versus kc/ω_c obtained from Eq. (34) (dashed curve) for $x_{\text{on}} = \alpha_{01}$ and $x_{\text{on}} R_0/R_w = \alpha_{11}$, and from Eq. (46) (solid curve) for $\epsilon = 1$, $R_w \omega_c/c = R_c \omega_c/c = \alpha_{01}/\gamma_z = 3.75$. Evidently, the growth rate calculated from the dispersion relation in Eq. (46), including beam self-dielectric effects, is only slightly larger than the growth rate obtained from the approximate dispersion relation in Eq. (34).

Stability boundaries in the parameter space $(R_c \omega_c/c, \epsilon)$ are illustrated in Fig. 9 for several values of $R_w \omega_c/c$ ranging from 2.2 to 2.8. In Fig. 9, the solid curves correspond to the stability boundaries obtained from Eq. (46) for $\hat{\gamma} = 1.118$ and $\beta_z = 0.4$. For a given value of $R_w \omega_c/c$, the region of $(R_c \omega_c/c, \epsilon)$ parameter space below the curve

corresponds to stability ($\chi_i = 0$) for arbitrary values of axial wavenumber k , whereas the region of parameter space above the curve corresponds to instability for some range of axial wavenumber.

Several points are noteworthy from Fig. 9. First, for general values of $R_w \omega_c / c$, the stability boundaries converge to the common value $R_c \omega_c / c \approx 3.6$ for $\epsilon = 1$, corresponding to the vacuum dielectric constant. Second, for a fixed inner radius R_w of dielectric material, the value of dielectric constant ϵ required for instability increases rapidly to infinity as the radius R_c of the conducting wall approaches the inner radius R_w . Third, for a given conducting wall radius R_c , instability occurs as the value of R_w is decreased, even for small values of $\epsilon - 1$.

The dependence of stability properties on dielectric constant ϵ is further illustrated in Fig. 10, where the normalized growth rate χ_i is plotted versus ϵ for $R_c \omega_c / c = 3.75$, $R_w \omega_c / c = 2.4$, $kc / \omega_c = 0.2$, $\hat{\gamma} = 1.118$, $\beta_1 = 0.4$ and $\nu = 0.002$. For these particular parameters, the maximum growth rate $\chi_i = 0.024$ occurs for dielectric constant $\epsilon = 1$. The range of ϵ exhibits instability bands as the value of dielectric constant ϵ is increased. For example, in Fig. 10, the system is unstable for ϵ satisfying $1 < \epsilon < 2.9$ (first radial harmonic number $n = 1$), $10.2 < \epsilon < 13.2$ (second radial harmonic number $n = 2$), etc. For the value of conducting wall radius ($R_c \omega_c / c = 3.75$) in Fig. 10, in the absence of dielectric material ($\epsilon = 1$), the system is unstable only for the first radial harmonic number $n = 1$. Since the addition of a dielectric material can significantly reduce the radial wavelength of the waveguide mode, it is possible to have high radial mode perturbations when the dielectric constant ϵ is large.

Carefully examining the cubic equation (46), and noting that $(1 + kc\beta_z/\omega_c)^2 > (kc/\omega_c)^2$ in the typical regime of interest, we conclude from Eq. (46) that either $(b_- + b_+)_{\omega_0} > 0$, or $|(b_- + b_+)_{\omega_0}| \ll 1$ for $(b_- + b_+)_{\omega_0} < 0$, are required for instability. Moreover, in order to have a smooth unstable spectrum with broad bandwidth, it is required that

$$|a| = \left| \frac{b_- + b_+}{\omega_c \frac{d}{d\omega} (b_- + b_+)} \right|_{\omega_0} \ll 0.1, \quad (47)$$

over a considerable range of k space when the beam is very tenuous ($v \ll 0.01$).

For present purposes, to illustrate the influence of dielectric material on instability bandwidth, shown in Fig. 11 are plots of (a) $(b_- + b_+)_{\omega_0}$, (b) the quantity a [Eq. (47)], and (c) the normalized growth rate χ_i versus kc/ω_c obtained from Eqs. (17), (18), (40), and (46) for $R_w\omega_c/c = 2.4$, $\hat{\gamma} = 1.118$, $\beta_1 = 0.4$, $v = 0.002$, and several values of $(R_c\omega_c/c, \epsilon)$. Several important features are noteworthy in Fig. 11. First, the matched geometric configuration with $(R_c\omega_c/c, \epsilon) = (3.75, 1)$ is the most unstable. However, the range of k -space corresponding to instability is relatively narrow. Second, the slightly unmatched configuration $(R_c\omega_c/c, \epsilon) = (3.75, 2)$ is unstable for a broad range of axial wavenumber k , with a considerably reduced growth rate. Moreover, the growth rate for $(R_c\omega_c/c, \epsilon) = (3.75, 2)$ is an abruptly varying function of wavenumber k . Evidently, from Fig. 11(b), the quantity a for $(R_c\omega_c/c, \epsilon) = (3.75, 2)$ does not satisfy Eq. (47). Third, we note from Fig. 11(b) that the quantity a for $(R_c\omega_c/c, \epsilon) = (3, 6)$ does satisfy Eq. (47), thereby resulting in a smooth growth rate curve with a broad bandwidth in k -space. Although the growth rate

for $(R_c \omega_c / c, \epsilon) = (3, 6)$ is slightly reduced from the case $(R_c \omega_c / c, \epsilon) = (3.75, 1)$, the range of k -space corresponding to instability is almost twice as broad. In this regard, the unstable spectrum for $(R_c \omega_c / c, \epsilon) = (3, 6)$ may be desirable for communication applications.

We conclude this section by emphasizing that cyclotron maser stability properties for a dielectric loaded waveguide exhibit a sensitive dependence on the value of ϵ and the thickness of the dielectric material. By appropriate choice of ϵ and thickness of dielectric material, it has been shown that the instability bandwidth can be increased more than a factor of two relative to a perfectly conducting waveguide, with only a slight reduction in growth rate.

VI. CONCLUSIONS

In this paper we have investigated the influence of finite wall impedance on the cyclotron maser instability for a hollow electron beam propagating in a waveguide with an arbitrary impedance Z . The stability analysis is carried out within the framework of the linearized Vlasov-Maxwell equations, assuming that the beam thickness is much less than the mean radius R_0 of the beam. The formal stability analysis for azimuthally symmetric electromagnetic perturbations ($\partial/\partial\theta = 0$) was carried out in Sec. II, including the important influence of finite wall impedance Z . In Sec. III, properties of the vacuum TE mode dispersion relation were investigated in the absence of the beam. A detailed analytic and numerical investigation of the cyclotron maser instability was carried out in Sec. IV for a wall impedance that is independent of frequency and axial wavenumber. One of the most important features of the analysis is the fact that, for a purely resistive wall, the growth rate is substantially reduced by introducing a very small amount of wall resistivity. Moreover, the range of kc/ω_c corresponding to instability increases rapidly as the resistivity of the wall is increased. Cyclotron maser stability properties in a dielectric loaded waveguide have been investigated in Sec. V. It is found that stability properties exhibit a sensitive dependence on the dielectric constant ϵ and thickness of the dielectric material. By appropriate choice of ϵ and thickness of dielectric material, the instability bandwidth can be more than double that for a perfectly conducting waveguide.

ACKNOWLEDGMENTS

This research was supported in part by the Naval Surface Weapons Center Independent Research Fund, and in part by the Office of Naval Research.

REFERENCES

1. H. S. Uhm, R. C. Davidson, and K. R. Chu, Phys. Fluids 21, 1866 (1978).
2. V. A. Flyagin, A. V. Gaponov, M. I. Petelin, and V. K. Yulpatov, IEEE Trans. Microwave Theory Tech. MTT-25, 514 (1977).
3. H. S. Uhm, R. C. Davidson, and K. R. Chu, Phys. Fluids 21, 1877 (1978).
4. P. Sprangle and A. T. Drobot, IEEE Trans. Microwave Theory Tech. MTT-25, 528 (1977).
5. H. S. Uhm and R. C. Davidson, Phys. Fluids 22, 1804 (1979).
6. K. R. Chu, Phys. Fluids 21, 2354 (1978).
7. H. S. Uhm and R. C. Davidson, Phys. Fluids 22, 1811 (1979).
8. E. Ott and W. M. Manheimer, IEEE Trans. Plasma Sci. PS-3, 1 (1975).
9. H. S. Uhm and R. C. Davidson, J. Appl. Phys. 50, 696 (1979).
10. J. L. Hirshfield, I. B. Bernstein, and J. M. Wachtel, IEEE J. Quantum Electron. QE-1, 237 (1965).
11. V. L. Granatstein, P. Sprangle, R. K. Parker, M. Herndon, and S. P. Schlesinger, J. Appl. Phys. 46, 3800 (1975).
12. N. I. Zaytsov, T. B. Pankratova, M. I. Petelin, and V. A. Flyagin, Radio Eng. Electron. Phys. 19, 103 (1974).
13. M. Friedman, D. A. Hammer, W. M. Manheimer, and P. Sprangle, Phys. Rev. Lett. 31, 753 (1973).
14. J. R. Pierce, Traveling-Wave Tubes, (D. Van Nostrand Company, Inc., New York, 1950) Chap. 4.
15. C. K. Birdsall and J. P. Whinnery, J. Appl. Phys. 24, 314 (1953).

FIGURE CAPTIONS

- Fig. 1 Contours of constant phase angle ϕ and modulus $|Z|$ [Eq. (22)] in the complex plane $x_{on} = (x_r, x_i)$ for (a) $n = 1$ and (b) $n = 2$.
- Fig. 2 Sketch of $\omega = (k^2 c^2 + \alpha_{on}^2 c^2 / R_w^2)^{1/2}$ versus k (corresponding to zero wall impedance), and $\omega = (k^2 c^2 + x_{on}^2 c^2 / R_w^2)^{1/2}$ versus k (corresponding to an arbitrary wall impedance Z). The straight line $\omega = k\beta_z c + \omega_c$ is the cyclotron resonance mode.
- Fig. 3 Plot of the normalized (a) growth rate χ_i and (b) Doppler-shifted real frequency χ_r versus kc/ω_c [Eq. (34)] for $\nu = 0.002$, $\hat{\gamma} = 1.118$, $\beta_{\perp} = 0.4$, $n = 1$, $R_o/R_w = 0.5$, $\phi = 90^\circ$, and several values of $|Z|$.
- Fig. 4 Plot of the normalized growth rate χ_i versus kc/ω_c for $|Z| = 0.05$, several values of phase angle ϕ , and parameters otherwise identical to Fig. 3.
- Fig. 5 Plot of normalized maximum growth rate (solid curve) and $R_o/R_w = \alpha_{11}/x_{on}$ (dashed curve) versus $x_{on} = x_r$ [Eqs. (36) and (35)] for parameters identical to Fig. 3.
- Fig. 6 Equilibrium configuration for a hollow electron beam in a dielectric loaded waveguide.
- Fig. 7 Plot of impedance Z versus ξ (dashed curves), and Z versus η (solid curves) [Eq. (44)] for $\zeta = 4, 5$, and 6 . The horizontal scale represents both of the variables ξ and η .
- Fig. 8 Plot of the normalized growth rate χ_i versus kc/ω_c obtained from the approximate dispersion relation in Eq. (34) (dashed curve) for $x_{on} = \alpha_{on}$ and $x_{on} R_o/R_w = \alpha_{11}$, and from the self-consistent dispersion relation in Eq. (46) (solid curve), for $\epsilon = 1$, $R_w \omega_c / c = R_o \omega_c / c = 3.75$.
- Fig. 9 Stability boundaries [Eq. (46)] in the parameter space $(R_o \omega_c / c, \epsilon)$ for $R_o \omega_c / c = \alpha_{11}$, several values of $R_w \omega_c / c$, and parameters

otherwise identical to Fig. 3.

Fig. 10 Plot of the normalized growth rate χ_i versus ϵ [Eq. (46)] for $R_c \omega_c / c = 3.75$, $R_w \omega_c / c = 2.4$, $R_o \omega_c / c = \alpha_{11}$, $kc / \omega_c = 0.2$, and parameters otherwise identical to Fig. 3.

Fig. 11 Plots of (a) $(b_- + b_+)_{\omega_o}$, (b) the ratio a , and (c) the normalized growth rate χ_i versus kc / ω_c [Eqs. (17), (18), (40), and (46)] for $R_w \omega_c / c = 2.4$, several values of $(R_c \omega_c / c, \epsilon)$, and parameters otherwise identical to Fig. 3.

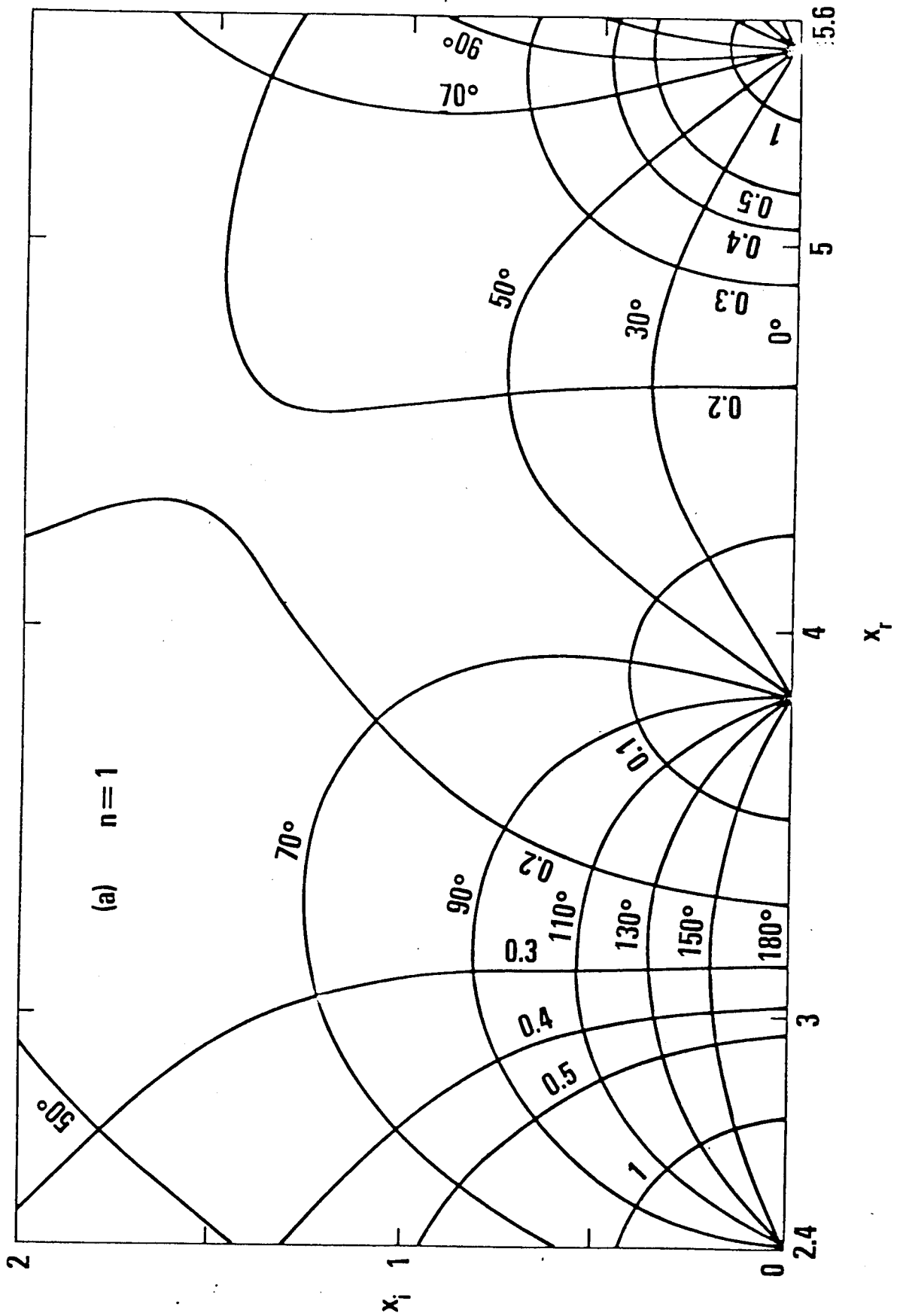


Figure 1a

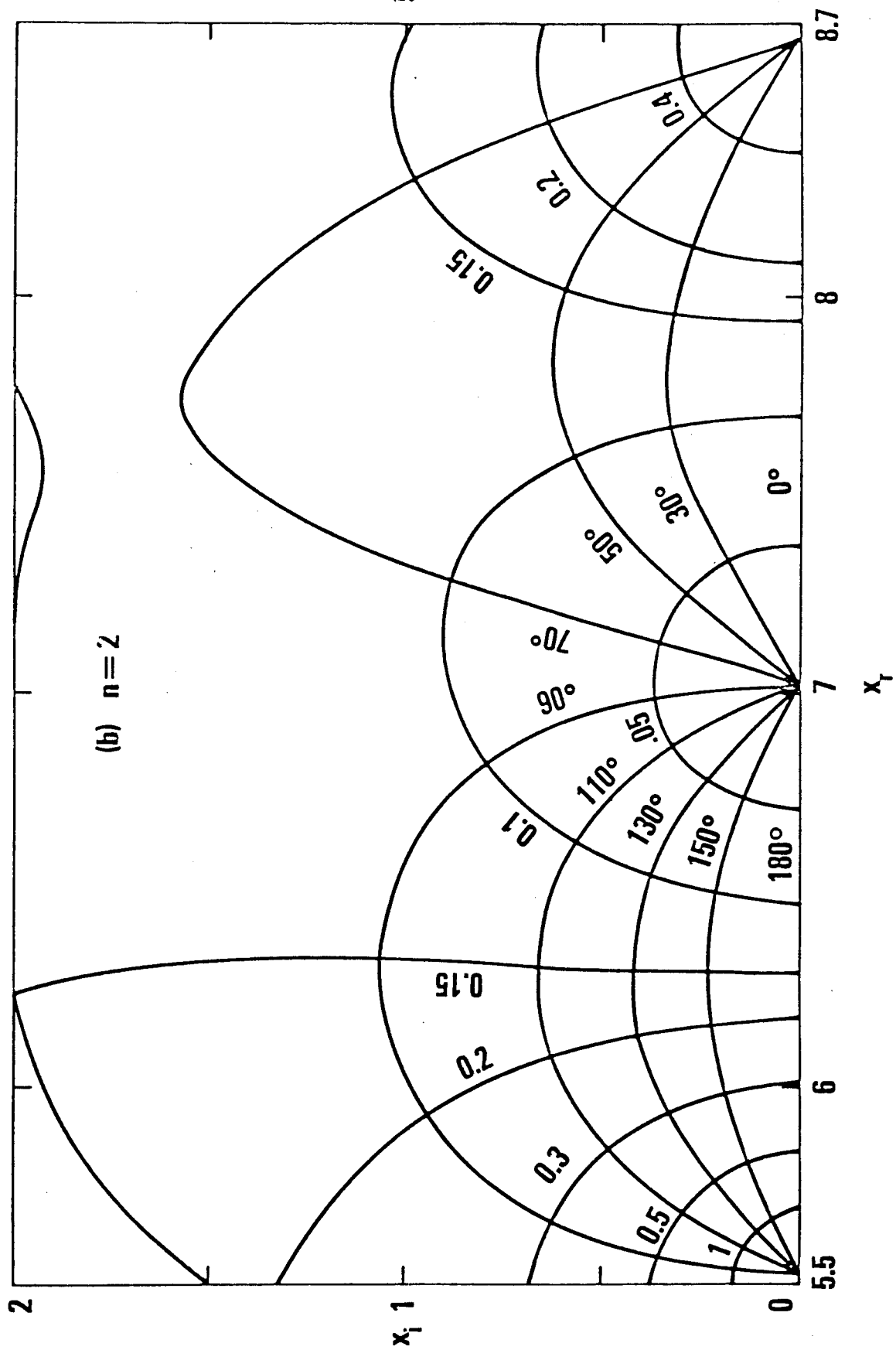


Figure 1b

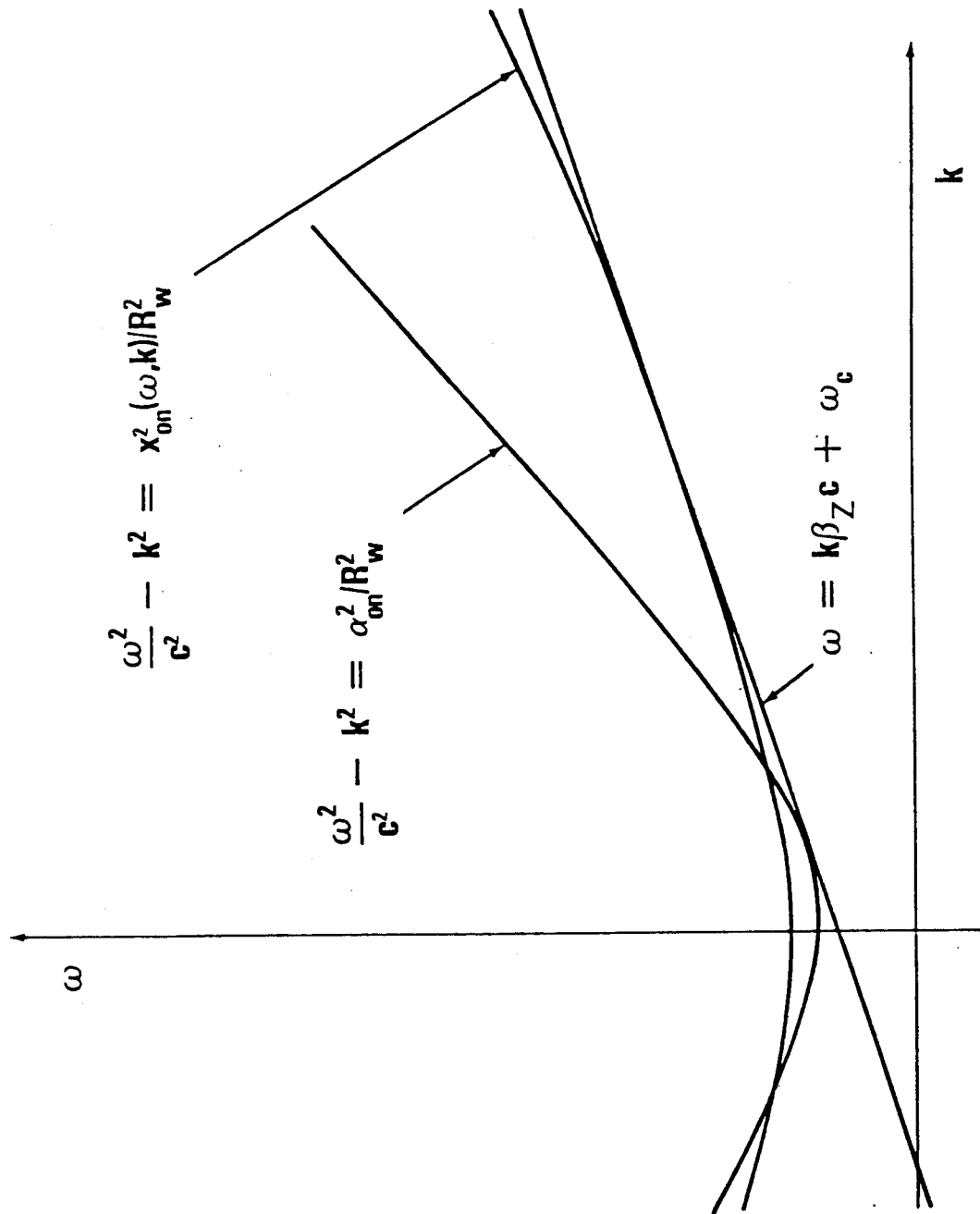


Figure 2

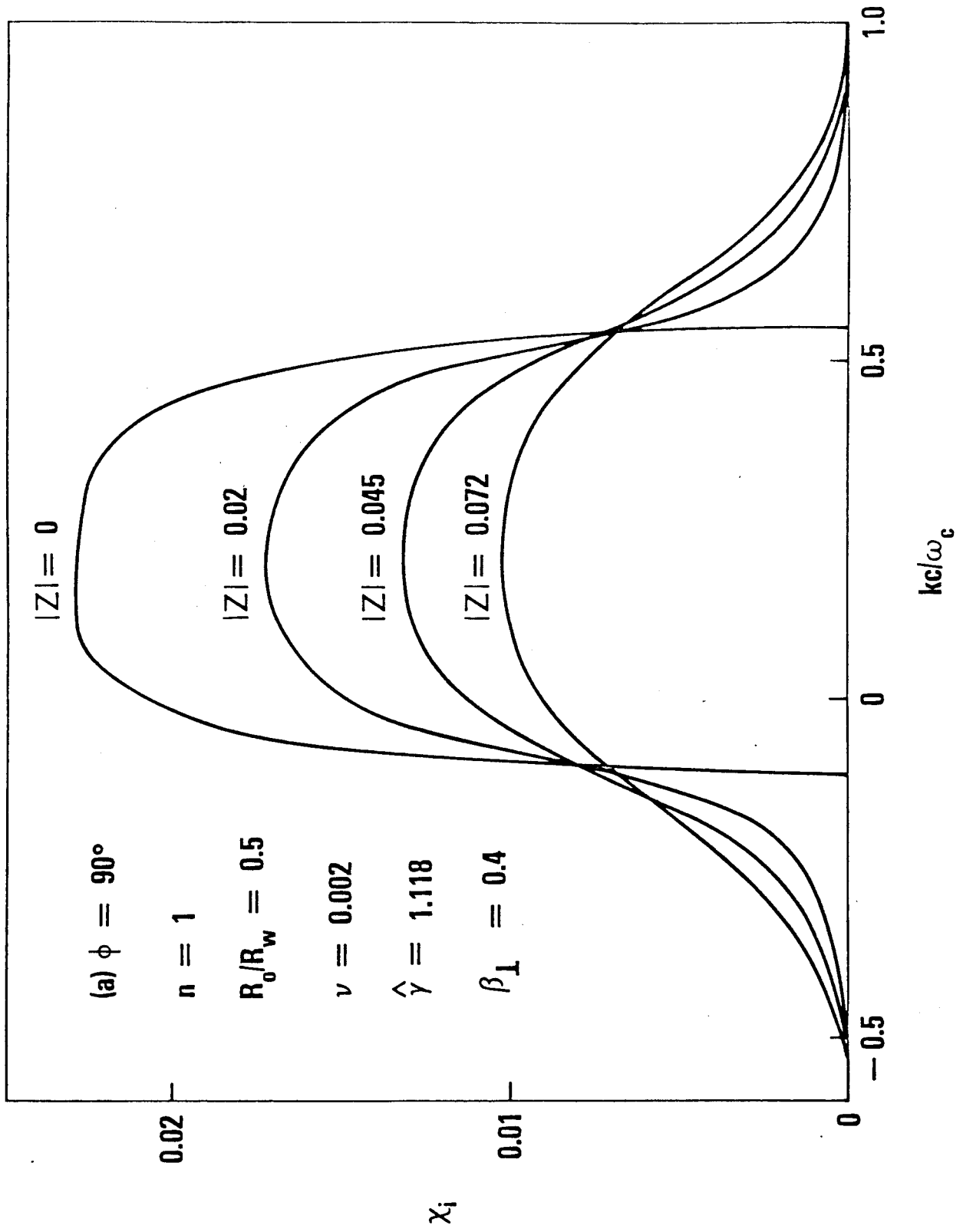


Figure 3a

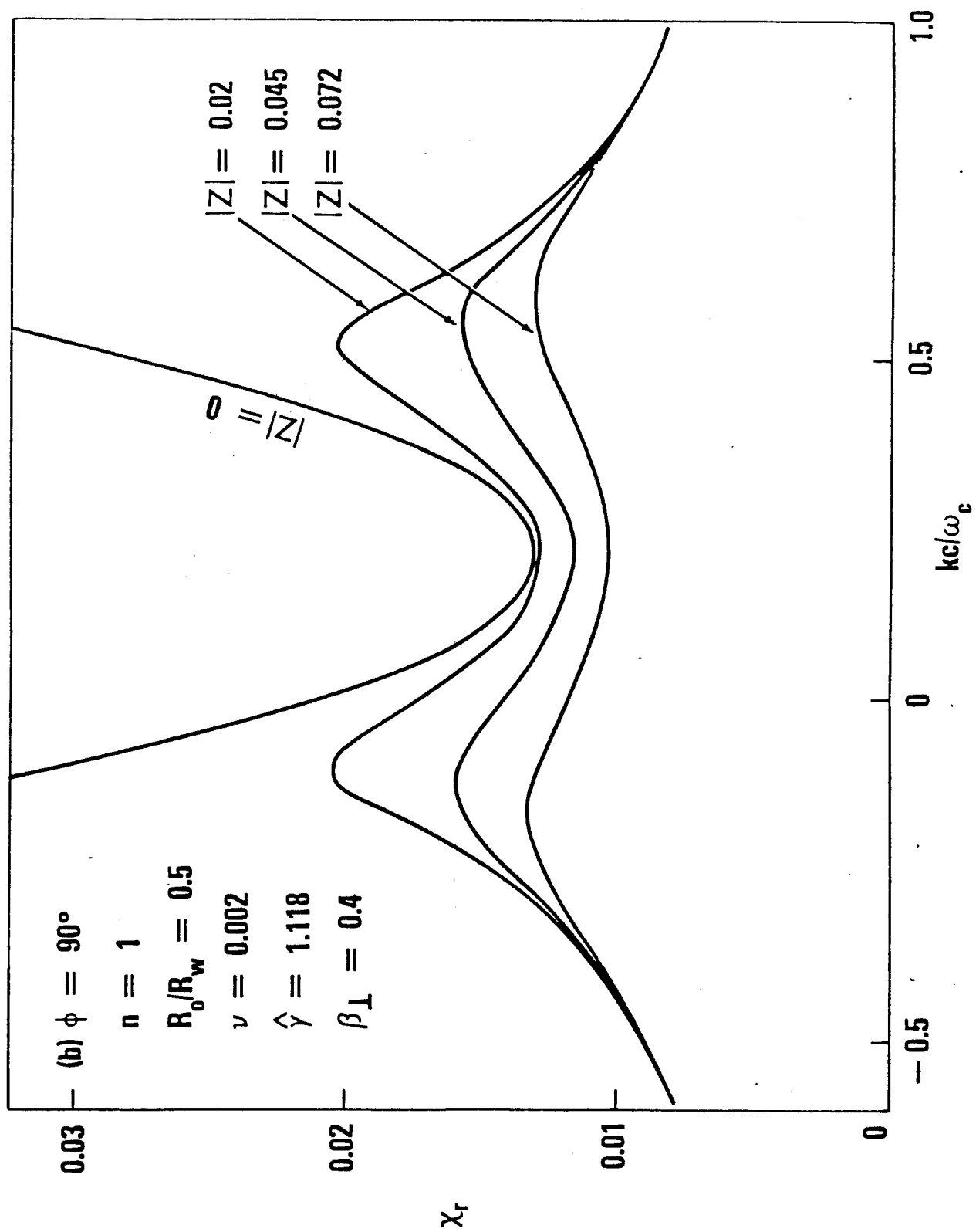


Figure 3b

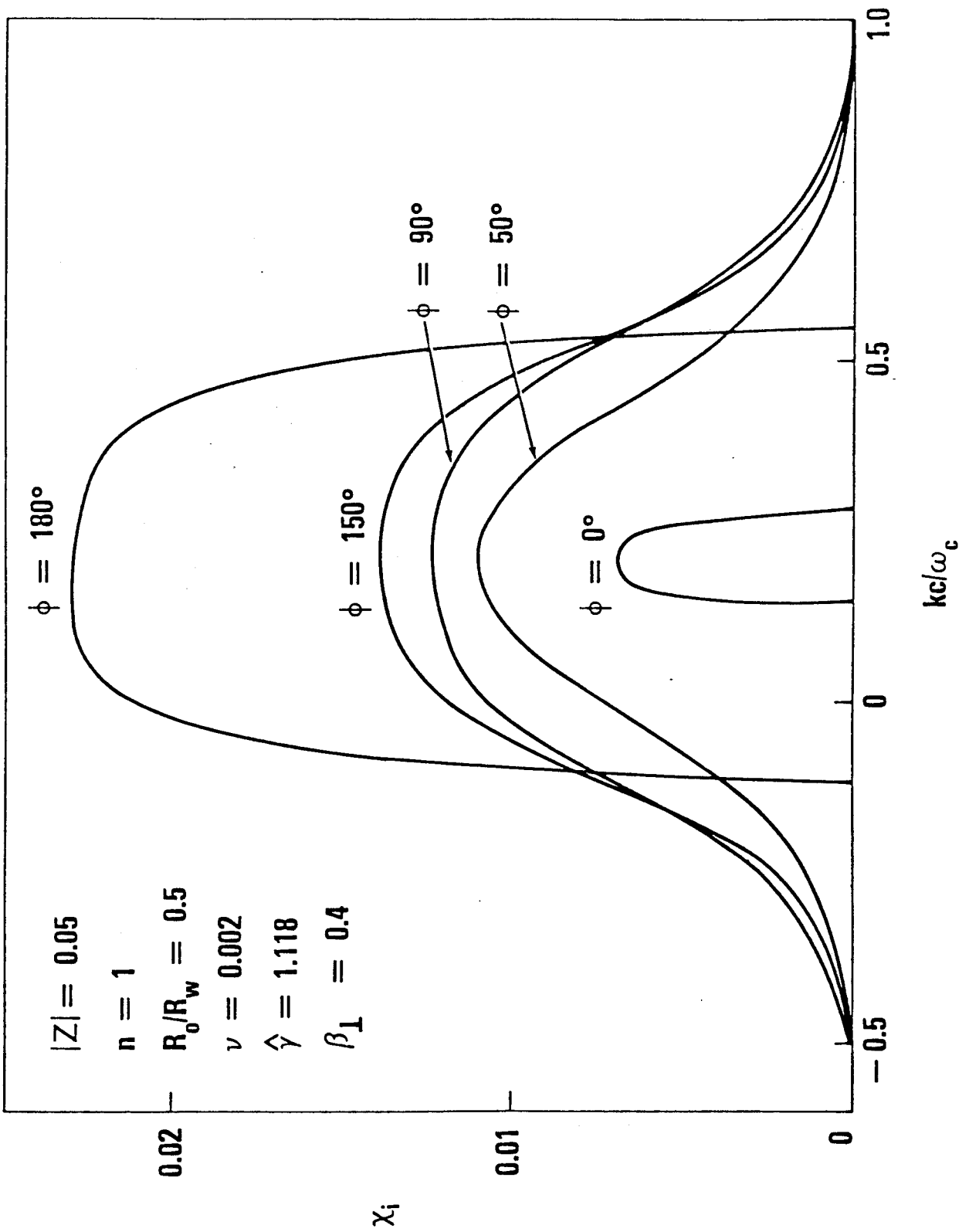


Figure 4

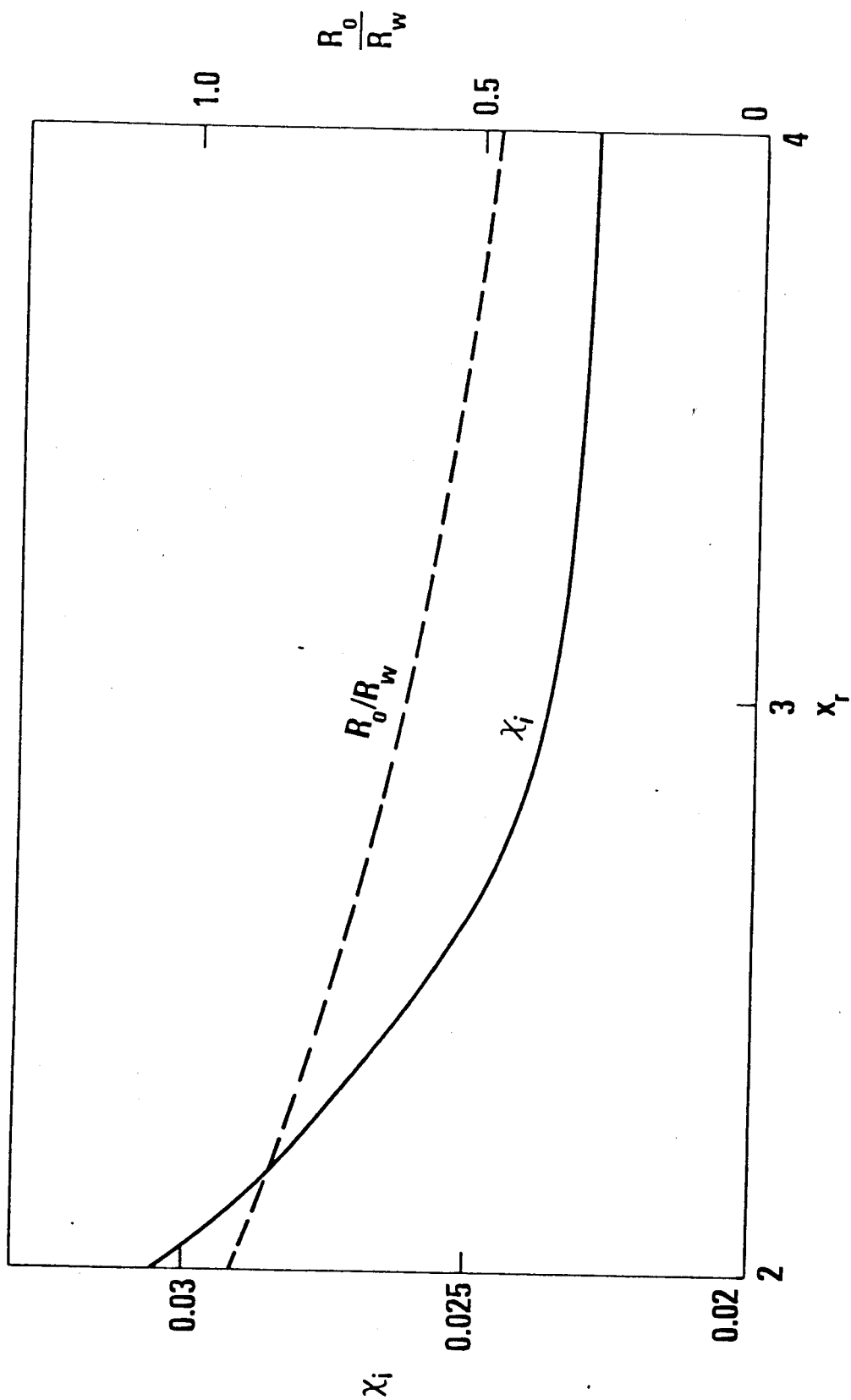


Figure 5

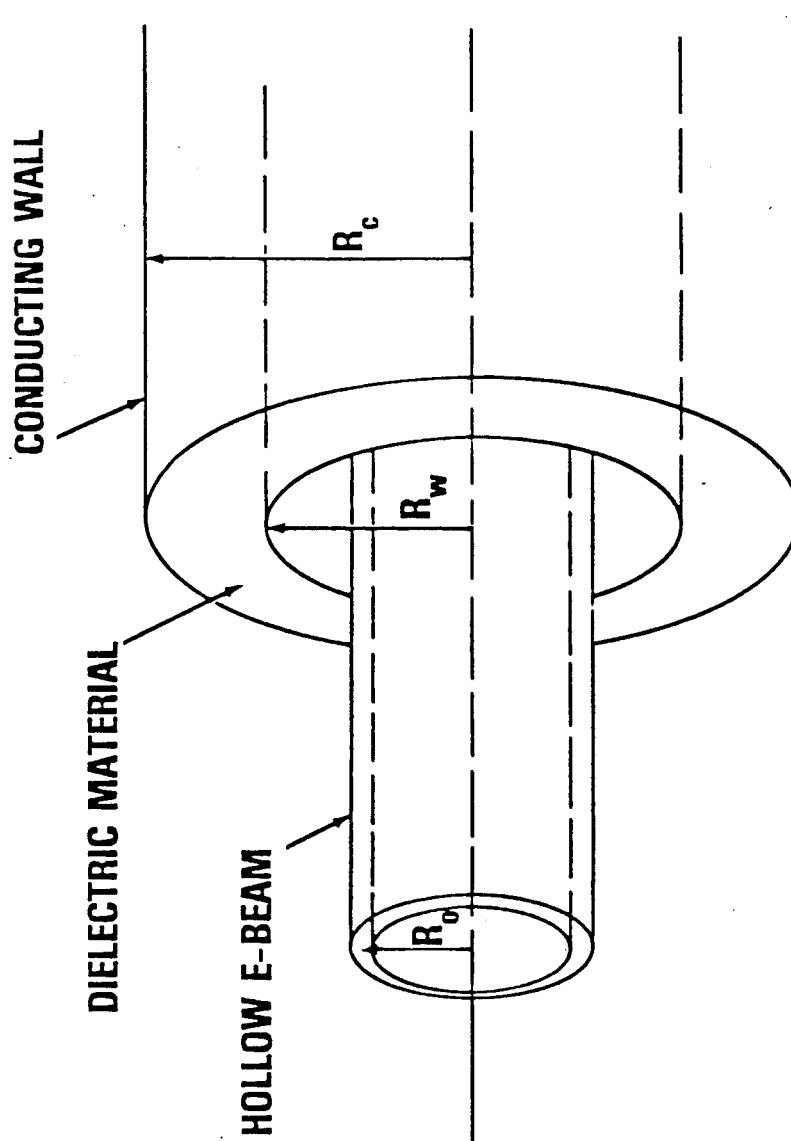


Figure 6

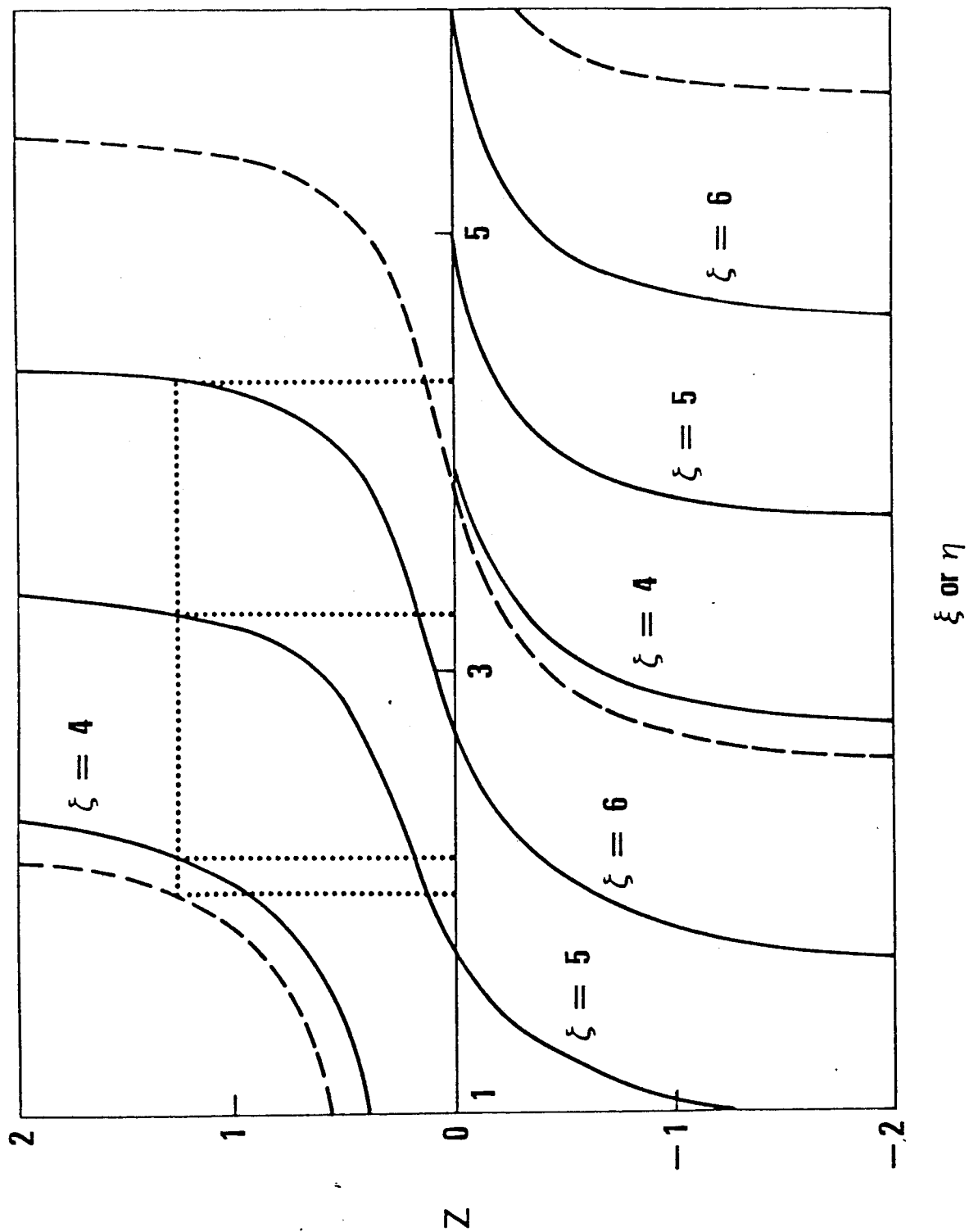


Figure 7

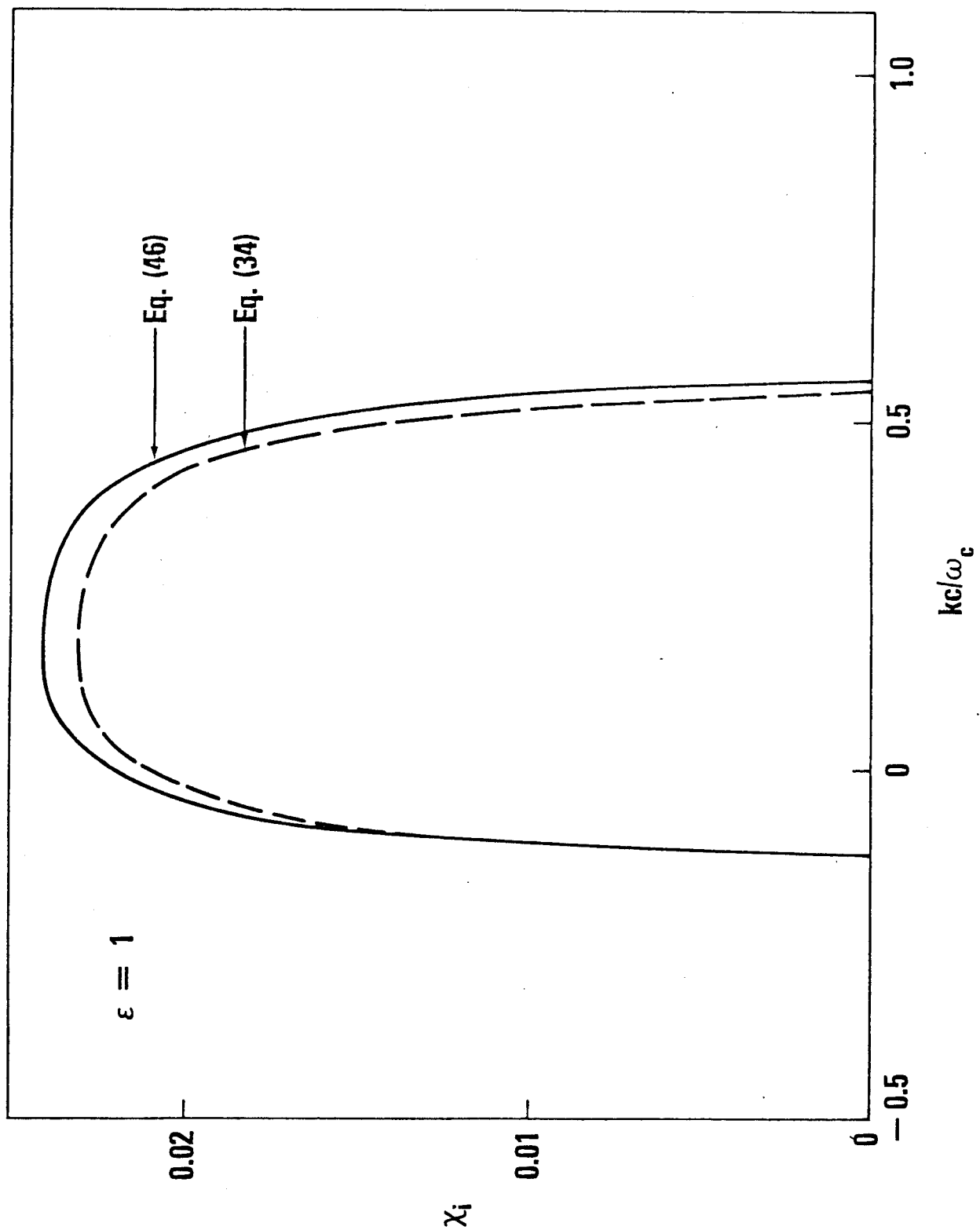


Figure 8

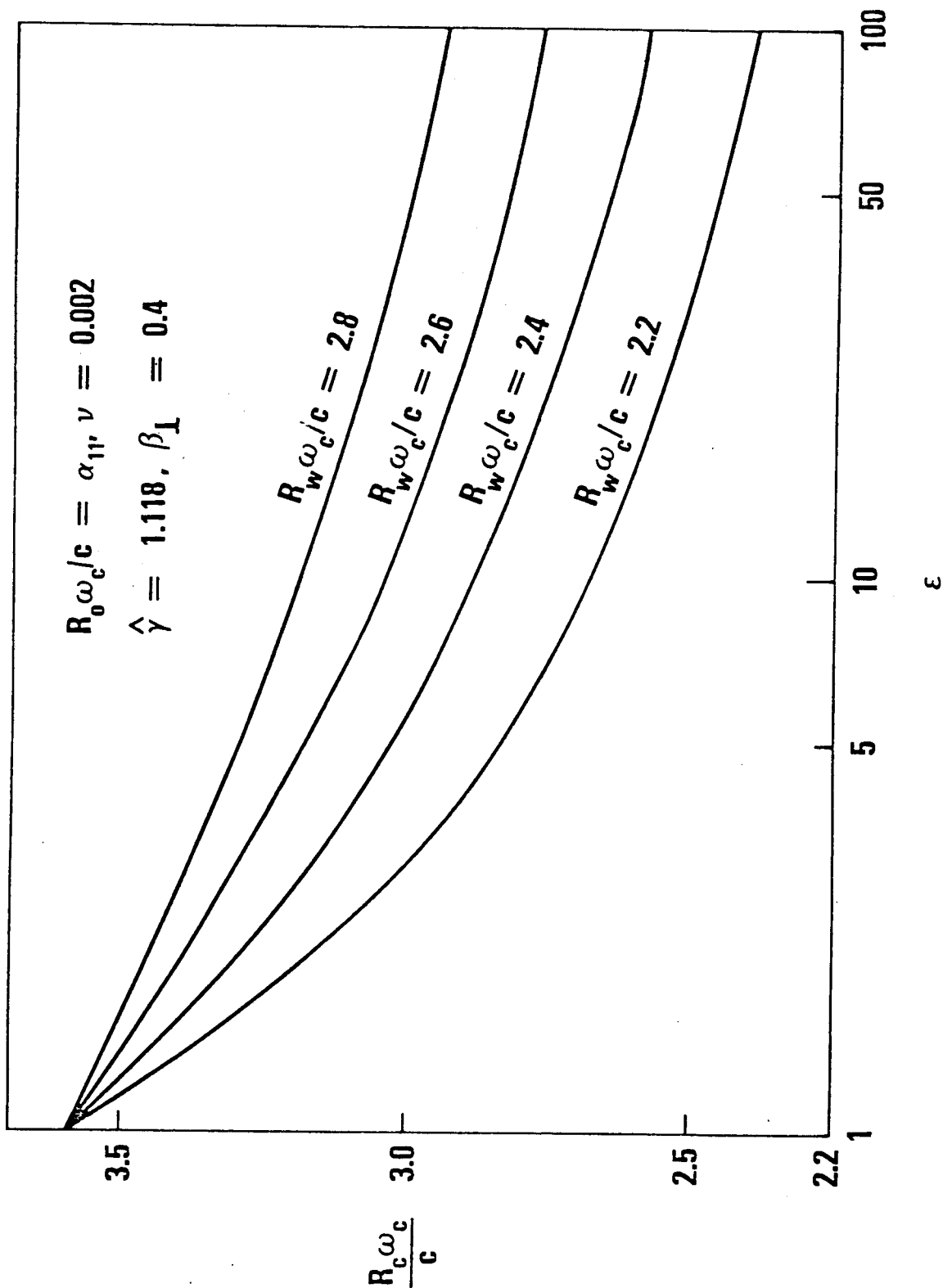


Figure 9

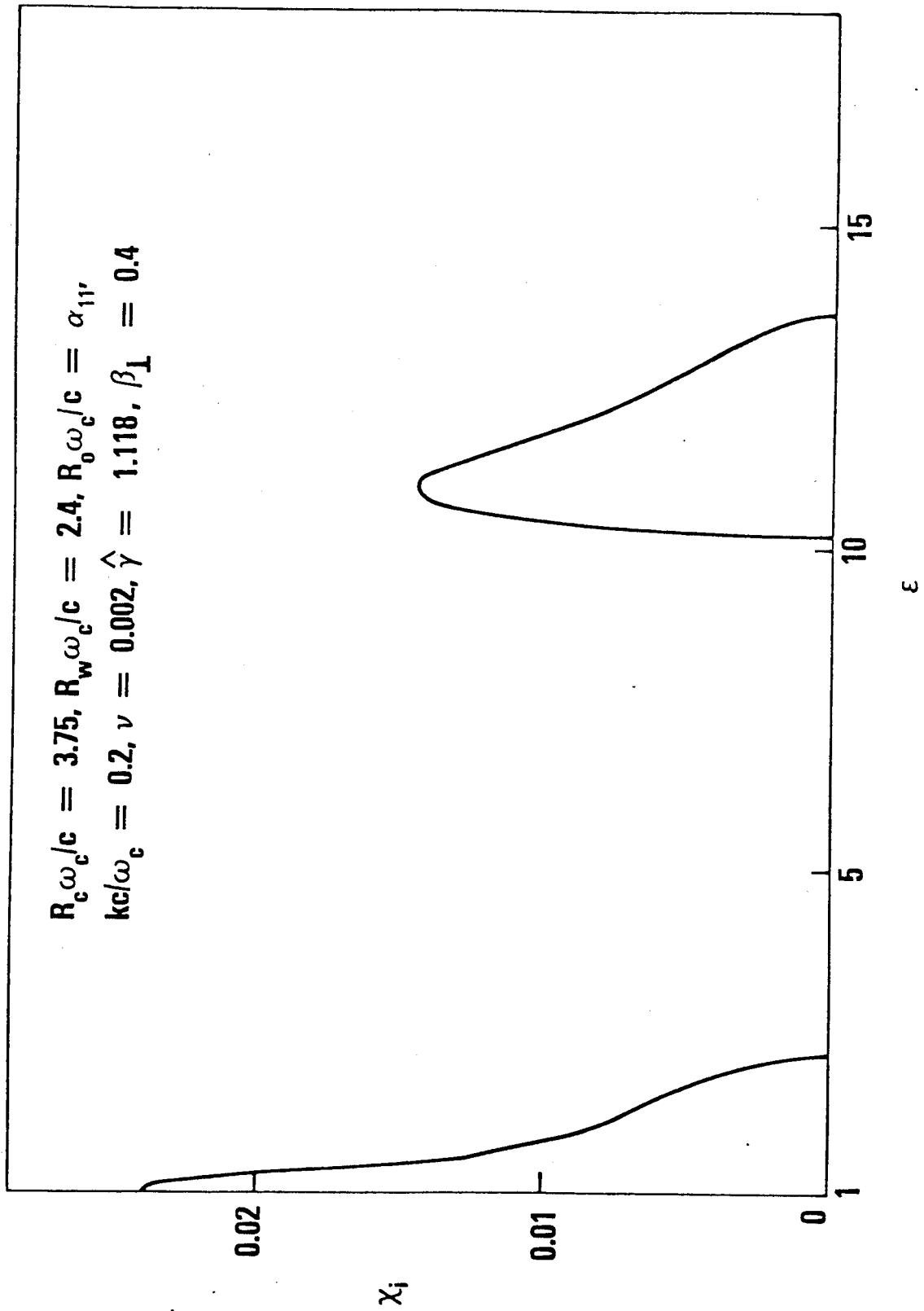


Figure 10

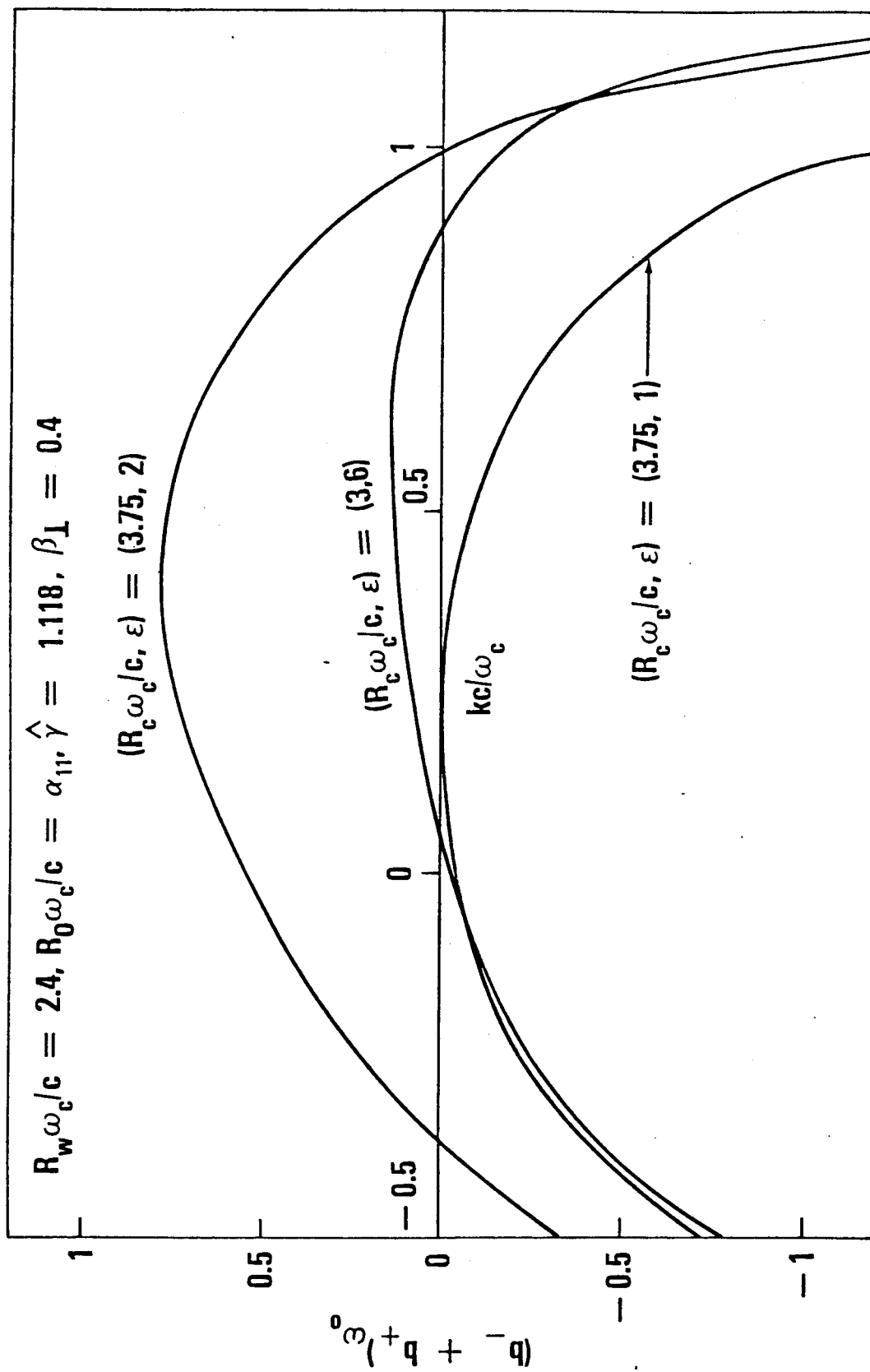


Figure 11a

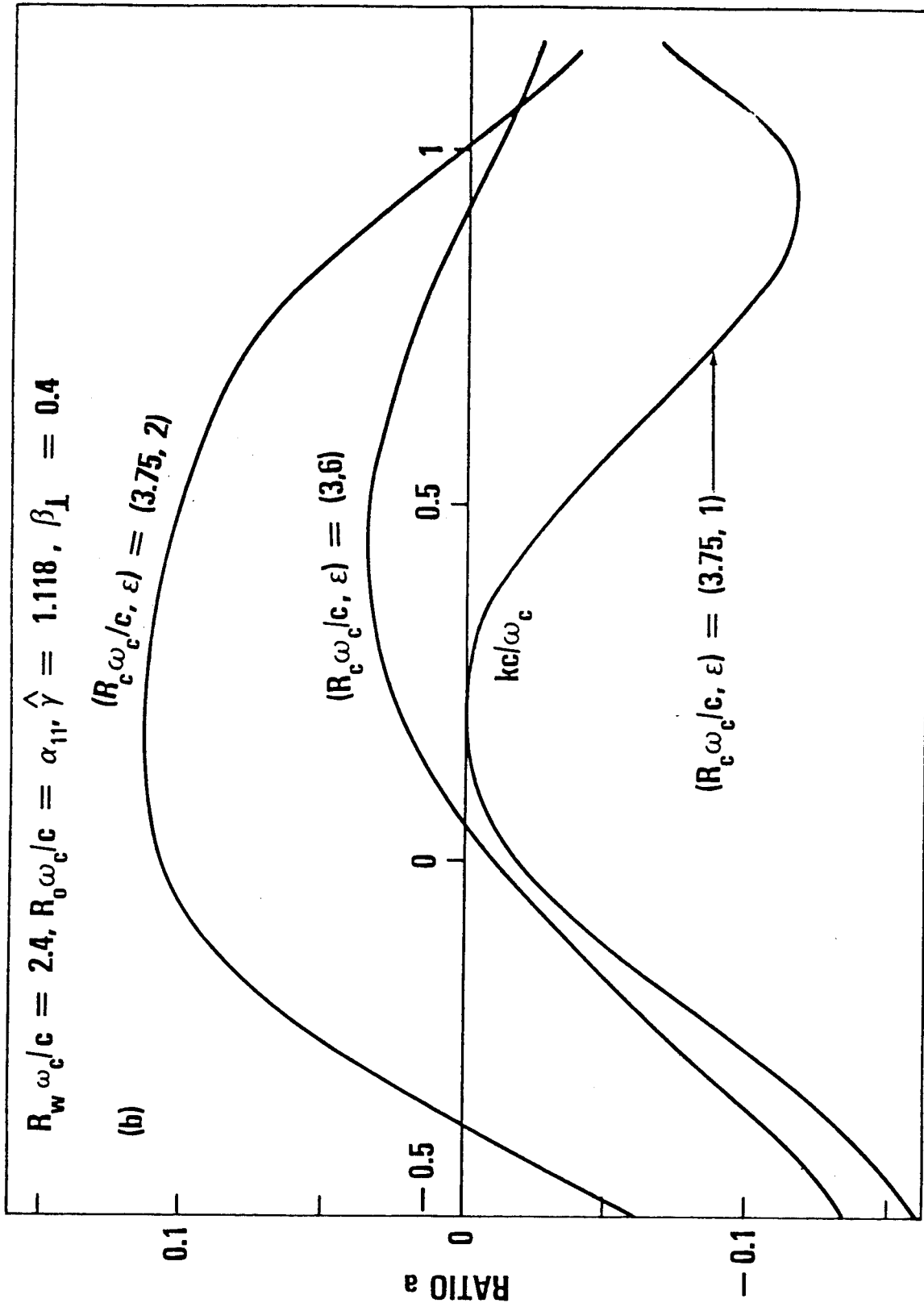


Figure 11b

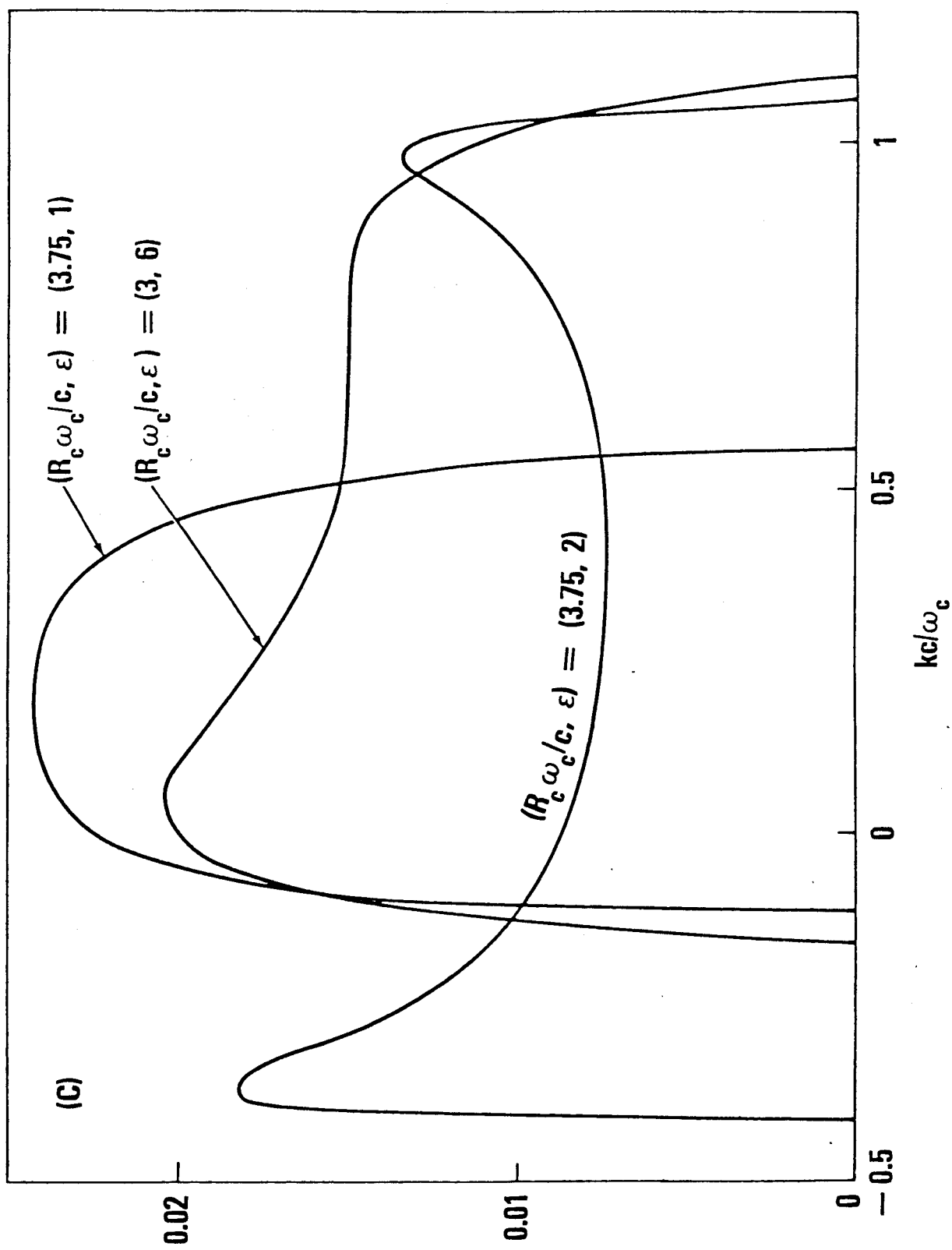


Figure 11c